




Cite this: *RSC Adv.*, 2023, **13**, 19096

# Enhancing the FRET by tuning the bandgap of acceptor ternary ZnCdS quantum dots

Muhammad Mubeen,<sup>a</sup> Noor ul Ain,<sup>a</sup> Muhammad Adnan Khalid,<sup>a</sup> Maria Mukhtar,<sup>a</sup> Bushra Naz,<sup>a</sup> Zumaira Siddique,<sup>a</sup> Anwar Ul-Hamid <sup>b</sup> and Azhar Iqbal <sup>\*a</sup>

In this article, we report the band gap tuning of ternary ZnCdS quantum dots (QDs) by varying the concentration of the capping ligand, mercaptoacetic acid (MAA). The functionalization of QDs leads to the control of their size and band gap due to the quantum confinement effect, causing blue shift in the absorption and photoluminescence (PL) spectra with a gradual change in the concentration of the capping ligand from 0.5 to 2.5 M. Ensulizole (2-phenylbenzimidazole-5-sulfonic acid) is an important organic ultraviolet (UV) filter that is frequently used in sunscreen cosmetics. An effective overlapping of the PL spectrum of ensulizole and the absorption spectrum of QDs with 2.5 M MAA is achieved. A formidable decrease in the PL intensity and the PL lifetime of ensulizole promotes an efficient Förster resonance energy transfer (FRET) from sunscreen ensulizole to the QDs. The magnitude of the FRET efficiency ( $E$ ) is  $\sim 70\%$ . This very high value of  $E$  is the signature of the existence of a very fast energy transfer process from ensulizole to the MAA functionalized ZnCdS QDs. The dyad system consisting of ZnCdS QDs and ensulizole sunscreen can serve as a prototype model to develop a better understanding of the photochemistry of ensulizole and consequently the formulation of more efficient sunscreen cosmetics.

Received 15th May 2023  
 Accepted 16th June 2023

DOI: 10.1039/d3ra03233g

[rsc.li/rsc-advances](https://rsc.li/rsc-advances)

## 1. Introduction

QDs exhibit fascinating optical and electronic properties in contrast to their bulk counterparts<sup>1</sup> due to the quantum confinement effect.<sup>2,3</sup> The novel properties of QDs can be concocted by regulating their size and composition *via* alloying and doping techniques.<sup>4,5</sup> The QDs based on metal chalcogenides of the main group II–VI have gained much importance in the fields of optoelectronics,<sup>6</sup> QD lasers,<sup>7</sup> heterojunction solar cells,<sup>8</sup> photodetectors,<sup>9,10</sup> photovoltaics,<sup>11</sup> biosensing,<sup>12</sup> biolabeling<sup>13</sup> and for linear and non-linear optical limiting properties<sup>14,15</sup> due to their tunable optical properties and size-tunable fluorescence emission.<sup>16</sup>

Recently, much attention has been devoted to the synthesis of binary,<sup>17</sup> ternary,<sup>18</sup> and core-shell type QDs.<sup>19</sup> Binary QDs of group II–VI have been proven to be potential candidates for solar cells, light-emitting diodes, and lasers, but ternary semiconductor QDs have compositional dependent optoelectronic properties *i.e.*, for instance, the PL emission and photoluminescence quantum yield (PLQY) can be tuned by varying their composition.<sup>20</sup> QDs with a binary composition have discrete bandgaps which limit their applications whereas

ternary QDs have continuously tunable bandgap energy.<sup>21</sup> Moreover, binary QDs mostly encompass toxic metals which also restrict their expediency. Nonetheless, ternary QDs are considered potential substitutes for binary QDs as they have high PLQY<sup>22</sup> with a low level of toxicity. The commonly used biocompatible ternary QDs involve AgInS, CuInS, and AgCuS.<sup>23,24</sup>

Among the ternary QDs, ZnCdS QDs have earned too much attention in recent decades due to the incredible dependency of bandgap (2.4–3.7 eV) on their size and composition.<sup>25,26</sup> The novel properties of ZnCdS QDs lie in between ZnS and CdS QDs. The formation of these alloyed QDs follows the Hume–Rothery rule.<sup>27</sup> The electronegativity of Zn and Cd is 1.6 and 1.7 with corresponding atomic sizes 142 pm and 161 pm respectively.<sup>26</sup> This slight difference in electronegativities (0.1) and atomic radii (12%) advocates a feasible combination between Zn and Cd in the formation of ZnCdS QDs.<sup>28</sup> By changing Zn/Cd ratio in ZnCdS QDs, the absorption and emission spectra can be tuned. An increase in Zn content decreases the size of ZnCdS QDs, which leads to a remarkable quantum confinement effect. The ZnCdS QDs occupy an important position in the application of photoconductive devices, photocatalysis, and heterojunction solar cells due to their broad bandgap.<sup>29</sup> The PLQY of ZnCdS nanocrystals can be optimized through the suitable adjustment of the composition of Zn in ZnCdS.<sup>30</sup> It is foreseeable that such alloyed QDs provide multiple possibilities for bandgap tailoring and find their extensive use in a variety of applications.<sup>31,32</sup>

<sup>a</sup>Department of Chemistry, Quaid-I-Azam University, Islamabad-45320, Pakistan.  
 E-mail: [aiqbal@qau.edu.pk](mailto:aiqbal@qau.edu.pk)

<sup>b</sup>Core Research Facilities, King Fahd University of Petroleum & Minerals, Dhahran 31261, Saudi Arabia



Moreover, QDs are generally considered to be toxic but their toxicity depends on their shape, size, and surface functionalization.<sup>33</sup> Also, the introduction of Zn reduces the toxicity of CdS and renders it more biocompatible and safe to use in cosmetic products. The experiments have revealed that the human skin is not labile for the penetration of commercially available QDs.<sup>34</sup> Therefore, the combination of these ternary QDs with ensulizole sunscreen can improve the efficiency of commercial sunscreens.

Ensulizole is a prominent UV-B (280–315 nm) type filter<sup>35</sup> frequently used in sunscreen cosmetic products. As QDs have a large absorption cross-section that can be tuned over a broad spectral region, therefore, the association between ensulizole and QDs may act as an imperative route of absorbed energy dissipation. This photo-absorbed energy transfer dynamics can be assessed *via* Förster resonance energy transfer (FRET) model.<sup>36</sup> The FRET is a non-radiative mode of energy transfer from an excited state donor to the ground state of proximate acceptor system.<sup>37</sup> The FRET is frequently used as a molecular ruler to gauge the distance in the biological systems.<sup>37,38</sup> The other applications of FRET include visualization of molecular interactions,<sup>39</sup> single molecule conformational dynamics,<sup>40</sup> and monitoring binding/unbinding events in biological systems.<sup>41</sup> Recently, the effect of size of CdS QDs as a FRET acceptor antagonist on a sunscreen donor has been reported.<sup>42</sup> Very recently, the work of Cowden *et al.*<sup>43</sup> reveals that the combination of two sunscreen molecules into one composite sunscreen forms a product with good stability towards UV light absorption and its dissipation in ethanol and bestows advantages over single-component of sunscreens.<sup>43</sup>

In this article, we investigate the surface modification of ZnCdS QDs by varying the concentration of capping ligand that tunes the photophysical properties of QDs. The concentration of capping ligand MAA is varied from 0.5 to 2.5 M to achieve the maximum overlapping between the PL emission spectrum of ensulizole and the absorption spectrum of QDs. These QDs act as FRET acceptor in conjunction with ensulizole donor as a model system for the study of dissipation of absorbed UV energy. The UV-absorbed energy transfer efficiency from

ensulizole sunscreen to the QDs is ~70%, which is significantly higher than the efficiencies of 67.3% (ref. 42) and 64.05% (ref. 44) reported in the previous works.

## 2. Experimental

### 2.1. Materials

Zinc sulfate dihydrate ( $\text{ZnSO}_4 \cdot 2\text{H}_2\text{O}$ ,  $\geq 98\%$ ), cadmium chloride pentahydrate ( $\text{CdCl}_2 \cdot 5\text{H}_2\text{O}$ , 99%), mercaptoacetic acid ( $\text{HSCH}_2\text{COOH}$ , 98%), sodium sulfide nonahydrate ( $\text{Na}_2\text{S} \cdot 9\text{H}_2\text{O}$ , 99.9%), and sodium hydroxide ( $\text{NaOH}$ ,  $\geq 99\%$ ) were obtained from Sigma-Aldrich. Ensulizole (98%) was procured from the Tokyo Chemical Industry (TCI). All chemicals were of analytical grade and were used without any further treatment. Deionized water was utilized as a solvent in all the measurements.

### 2.2. Synthesis

The ZnCdS QDs were synthesized by employing the colloidal method.<sup>45,46</sup> Briefly, 0.1 M cationic precursors  $\text{ZnSO}_4 \cdot 2\text{H}_2\text{O}$  and  $\text{CdCl}_2 \cdot 5\text{H}_2\text{O}$  were prepared separately in deionized water and then taken into a three-necked round bottom flask along with 0.5 M MAA. The reaction mixture was stirred at 300 rounds per minute (RPM) and heated at 80 °C temperature under an inert atmosphere of nitrogen gas. To hold the pH of the solution between 9 and 11, NaOH solution (1 M) was added drop by drop. When the solution turned transparent, anionic precursor  $\text{Na}_2\text{S} \cdot 9\text{H}_2\text{O}$  (0.1 M) was added. The whole reaction mixture was heated and stirred for about one hour. The final solution was precipitated with ethanol and then isolated through ultracentrifugation. The obtained crystals of QDs were washed repeatedly with a mixture of ethanol and water to remove unreacted ingredients and finally dried at 50 °C in the oven for 6–7 hours. Similarly, the whole reaction procedure was repeated with other concentrations of MAA *i.e.* 1.0 M, 1.5 M, 2.0 M, and 2.5 M. Moreover, 5 mL of 85  $\mu\text{M}$  ensulizole was mixed with 1 mL of 133  $\mu\text{M}$  of ZnCdS QDs in a round bottom flask and stirred for 30 minutes at 60 °C for the effective association of the QDs with the ensulizole. The resultant solution was used as such for the FRET measurements. The molar concentration of QDs was measured

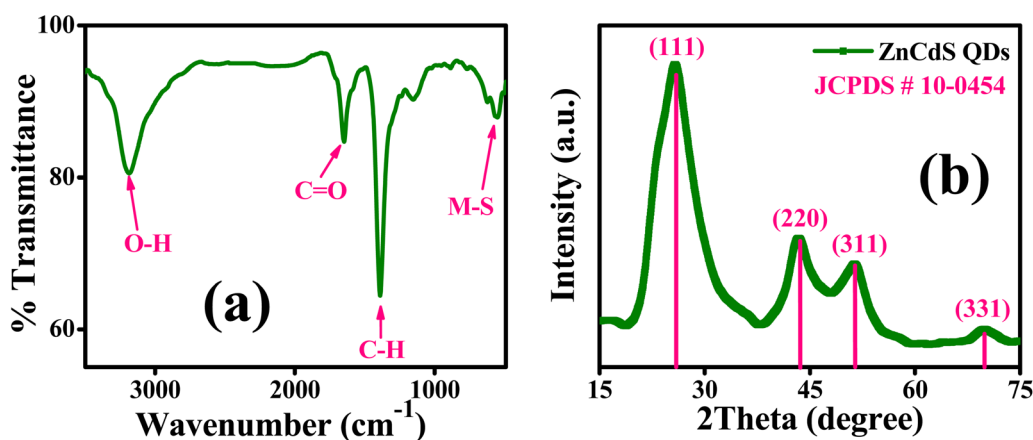


Fig. 1 (a) FTIR spectrum, and (b) XRD pattern of MAA (2.5 M) functionalized ZnCdS QDs.

by dividing the total volume per liter of the QDs by the volume of single QD, which was assessed from TEM micrograph (Fig. 2(b)). For the determination of total volume per liter of QDs, it was believed that both the nano and bulk materials had same density.<sup>47</sup> Afterward, the molar absorption coefficient of QDs was estimated from the slope of the line by plotting absorption verses concentrations as mentioned in our previously reported work.<sup>44</sup>

### 2.3. Characterization techniques

To confirm the functionalization of the synthesized ZnCdS QDs, Fourier transform infrared (FTIR) spectroscopic analysis is performed in the region between 4000 and 500  $\text{cm}^{-1}$  by using a BRUKER TENSOR-II FTIR spectrometer. The crystal structure of ZnCdS QDs is determined by using PANalytical X-ray diffractometer (XRD) model 3040/60 X'Pert PRO operated at 45 kV and 40 mA, having  $\text{CuK}_\alpha$  ( $\lambda = 1.54 \text{ \AA}$ ) as the radiation source over an angle range of  $10\text{--}80^\circ$  at a step size of  $0.02^\circ$ . The UV-Vis absorption measurements are performed with the help of the Shimadzu-1601 spectrophotometer in the wavelength range of 200–800 nm. The elemental analysis and particle size investigation of synthesized ZnCdS QDs are performed by JSM-6460 LV energy dispersive X-ray (EDX) and high-resolution transmission electron microscope (TEM), Philips CM 30, JEOL, JEM-2100F. Steady-state photoluminescence (SSPL) and time-resolved photoluminescence (TRPL) measurements are recorded by employing the PicoQuant, Germany, FluoTime 300 (FT-300) time-correlated single-photon counting (TCSPC) setup. The PL measurements of the samples are performed at room temperature after pulsed excitation at 306 nm with a pulsed

LED laser coupled to a TCSPC setup. The pulse duration of PLS-300 is 416 ps and pulse energy is 0.077 pJ. The long-pass color filter FGL400 is applied to filter the residual light of the excitation source and to elude the second-order of 306 nm.

## 3. Results and discussion

FTIR analysis is performed to detect different functional groups present in the sample of MAA capped ZnCdS QDs as depicted in Fig. 1(a). No characteristic peak is observed between the regions  $2550\text{--}2620 \text{ cm}^{-1}$  for S–H stretching mode that indicates the existence of strong binding interaction between the sulfur of the thiol group (S–H) of capping ligand to the surface of ZnCdS QDs. Hence, it can be inferred that ZnCdS QDs are successfully functionalized by MAA. The characteristic peaks that existed at  $3190 \text{ cm}^{-1}$  and  $1648 \text{ cm}^{-1}$  are attributed to the O–H and C=O bond stretching vibrations of the carboxylic group of capping ligand, respectively. The strong peak centered at  $1388 \text{ cm}^{-1}$  corresponds to the H–C–H bending mode. The typical peak observed at  $560 \text{ cm}^{-1}$  can be assigned to the stretching vibration modes of the metal–sulfur bond of ZnCdS.

The powder XRD technique is used to determine the crystal structure and crystallinity along with the crystallite size of the synthesized material. The XRD pattern of 2.5 M ZnCdS QDs along with the reference card is displayed in Fig. 1(b). This pattern matches with the crystal structure of the cubic zinc blende and is confirmed by JCPDS-10-0454. The four distinct peaks appeared at  $2\theta$  values of  $25.8^\circ$ ,  $43.6^\circ$ ,  $51.4^\circ$ , and  $70.0^\circ$  are associated with (111), (220), (311), and (331) crystal planes, respectively. The plane indexed with (111) is the most intense

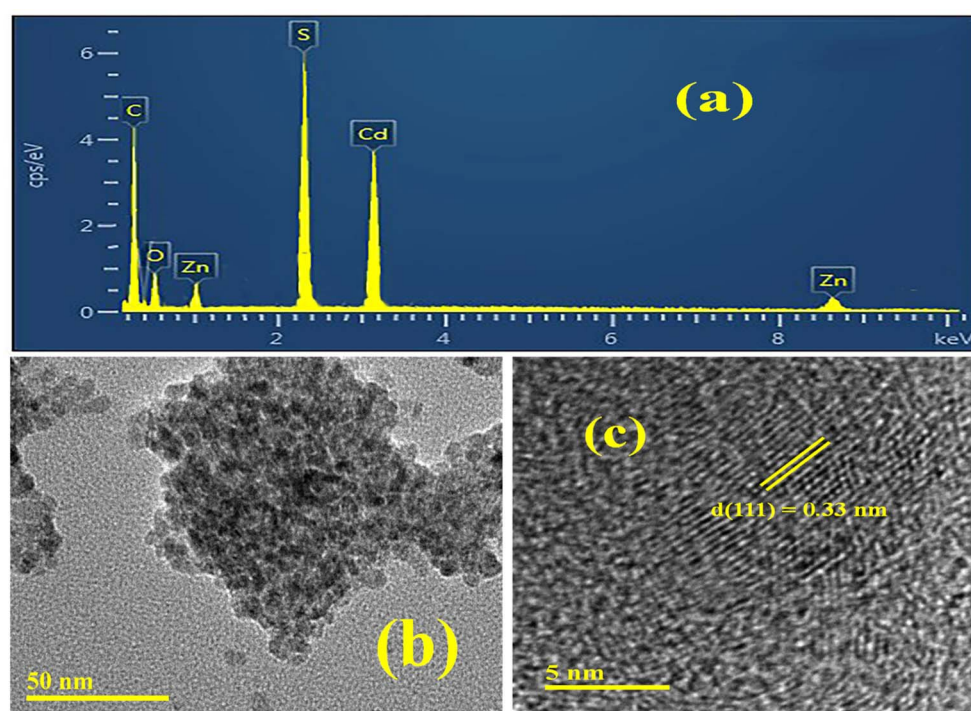


Fig. 2 (a) EDX analysis, (b) TEM micrograph, and (c) HRTEM micrograph of MAA (2.5 M) functionalized ZnCdS QDs.



peak and the manifestation of two closely spaced reflection planes (220) and (311) verify the crystalline nature of synthesized ZnCdS QDs. The crystallite size of 2.5 M MAA functionalized ZnCdS QDs is determined  $\sim 4.9$  nm with the help of Scherrer's eqn (1).

$$D = \frac{K\lambda}{\beta \cos \theta} \quad (1)$$

where  $D$ ,  $k$ ,  $\lambda$ ,  $\beta$  and  $\theta$  are crystallite size, Scherrer's constant (0.94 for cubic crystal structure), the wavelength of X-rays used, full width at half maximum, and Bragg angle respectively. The purity of the synthesized material is confirmed by EDX analysis as depicted in Fig. 2(a). To further verify the particle size of synthesized QDs, TEM measurements are performed and the images are displayed in Fig. 2(b). The particle size estimated from the TEM micrograph using ImageJ software is  $\sim 5$  nm which is in good concurrence with the crystallite size evaluated from the aforementioned eqn (1). The high-resolution TEM micrograph (Fig. 2(c)) unveils the crystal lattice parameters of the synthesized ZnCdS QDs, which corresponds to a  $d$ -spacing of 0.33 nm of the (111) crystal plane.

Fig. 3(a) displays UV-Vis absorption spectra of ZnCdS QDs with different concentrations of the functionalizing ligand (MAA). The ZnCdS QDs having a wide range of absorption edge lies in between bulk ZnS (3.62 eV)<sup>48</sup> and CdS (2.42 eV).<sup>49</sup> By increasing the concentration of capping ligand MAA, the blue shift in the first absorption exciton peak of QDs is a clear manifestation of the quantum confinement effect. Moreover, when the concentration of the capping ligand increases, more sites of QDs are engaged that decrease the nucleation and the size decreases. A blue shift is observed in absorption spectra that corresponds to an increase in bandgap energy that is estimated from Tauc's method and is displayed in Fig. 3(b).

As reflected in Fig. 3(b), the value of bandgap energy for ternary ZnCdS QDs comprising different concentrations of MAA varies linearly *i.e.* with the increase in the concentration of capping ligand from 0.5 M to 2.5 M, the value of the bandgap energy of QDs also increases from 2.88 eV to 3.37 eV, respectively. This again can be ascribed to the quantum confinement prodigy. The observation of this wide range in tunability of

bandgap energy of ternary ZnCdS QDs in contrast to binary ZnS and CdS can also be attributed to the composition of alloyed QDs along with the quantum size effect.<sup>50</sup>

From bandgap data, the average particle size of all the synthesized ZnCdS QDs is determined by applying Brus equation<sup>51</sup> eqn (2).

$$E_g^* = E_g + \frac{h^2}{8r^2} \left( \frac{1}{m_o m_e} + \frac{1}{m_o m_h} \right) - \frac{1.8e^2}{4\pi\epsilon_r\epsilon_o r} \quad (2)$$

where,  $E_g^*$  and  $E_g$  are the bandgap energies of QDs and bulk material, respectively.  $r$  is the radius of QDs,  $h$  is Planck's constant,  $m_e$  is the effective mass of the electron ( $0.2 m_o$ ),  $m_h$  is the effective mass of hole ( $0.8 m_o$ ),  $m_o$  is the rest mass of the free electron ( $9.11 \times 10^{-31}$  kg),  $\epsilon_r$  is relative dielectric constant (5.7  $\epsilon_o$ ),  $\epsilon_o$  is the dielectric constant of the vacuum ( $8.85 \times 10^{-12}$  C<sup>2</sup> N<sup>-1</sup> m<sup>-2</sup>) and  $e$  is the standard charge on an electron ( $1.6022 \times 10^{-19}$  C). The particle sizes of QDs in terms of diameter estimated from eqn (2) are 7.8 nm, 7.0 nm, 6.0 nm, 5.4 nm, and 5.1 nm for 0.5 M, 1.0 M, 1.5 M, 2.0 M, and 2.5 M MAA functionalized ZnCdS QDs, respectively.

Fig. 4(a) exhibits the SSPL spectra of ternary ZnCdS QDs with PL emission peaks centered at 590 nm, 573 nm, 552 nm, 516 nm, and 468 nm for 0.5 M, 1.0 M, 1.5 M, 2 M, and 2.5 M concentrations of capping ligand MAA, respectively. As the concentration of MAA increases, a blue shift in PL emission peak due to the quantum confinement effect is noticed which is in accordance with the UV-Vis absorption measurements of ZnCdS QDs as displayed in aforementioned Fig. 3(a). This gradual shift in PL emission peak with change in concentration of capping ligand MAA is also an indication of successful synthesis of assorted sized ZnCdS QDs. The extended PL tail towards the longer wavelengths of QDs containing the higher conc. of MAA can be attributed to the presence of trap states, which are accountable to cause defects such as dangling bonds and vacancies on the surface of the QDs.

The TRPL measurements are performed to get information about the PL decay kinetics of ZnCdS QDs. The PL decay kinetics demonstrate an excellent trend in the lifetime for differently sized functionalized ZnCdS QDs as evident from Fig. 4(b). Moreover, the shape of all the curves of Fig. 4(b)

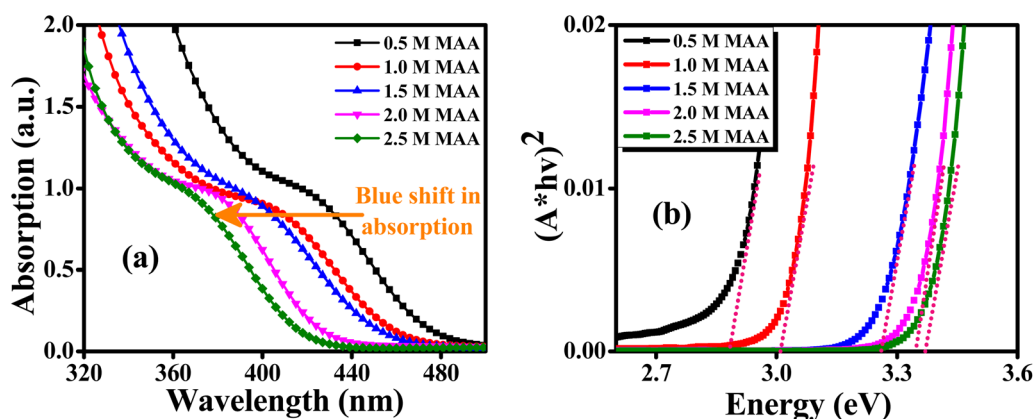


Fig. 3 (a) UV-Visible absorption spectra and (b) Tauc's plot of ZnCdS QDs functionalized with different concentrations of MAA.





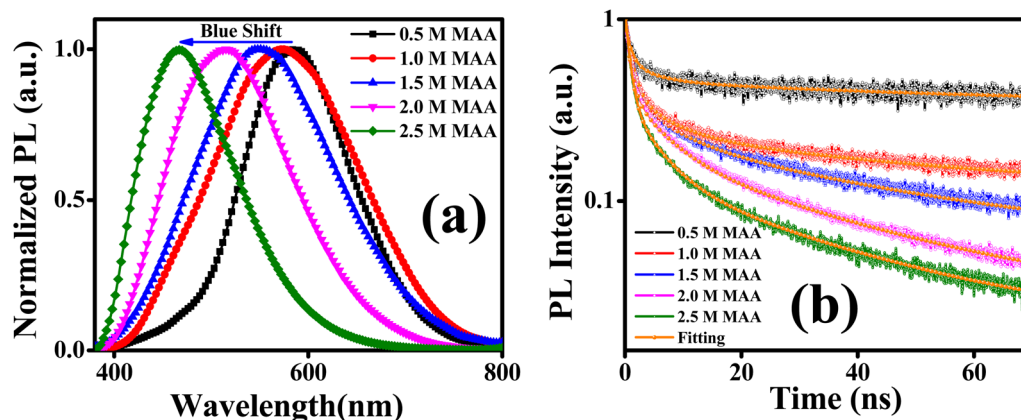


Fig. 4 (a) Normalized SSPL spectra, and (b) PL decay kinetics of ZnCdS QDs functionalized with different concentrations of MAA.

reveals that the 1st order decay kinetics is operative. The measured data is best fitted by tri-exponential decay function for the PL kinetics of different sized ZnCdS QDs. The various fitting parameters extracted from the best fits are shown in Table 1. The average PL decay lifetimes ( $\tau_{\text{average}}$ ) are calculated by employing eqn (4) using the time constants and the coefficients extracted from eqn (3).

$$Y = Y_0 + \sum_{i=1}^n A_i e^{-\frac{x}{t_i}} \quad (3)$$

$$\tau_{\text{average}} = \frac{A_1 \tau_1 + A_2 \tau_2 + A_3 \tau_3}{A_1 + A_2 + A_3} \quad (4)$$

here  $A_i$  and  $t_i$  are the associated coefficients and the time constants, respectively.

The average PL lifetime of ZnCdS QDs with 0.5 M MAA is 12.13 ns and as the concentration of MAA increases, PL lifetime decreases accordingly as evident from Table 1. The longest PL lifetime is observed with the 0.5 M concentration of MAA, this is because, for large-sized QDs, energy levels are more closely spaced in which electron and hole can easily be trapped, consequently, exciton in large-sized QDs exists for a longer period than in small-sized QDs.<sup>52</sup> Therefore, an increase in the concentration of MAA capping ligand results in the decrease in particle size of QDs, which leads to the creation of shallow trap states and subsequently, shortening of PL lifetime as displayed in Fig. 5.

Table 1 Fitting parameters extracted from the best fits of the measured PL decay kinetics for various MAA functionalized ZnCdS QDs

Conc. of MAA	$A_1$	$\tau_1$ (ns)	$A_2$	$\tau_2$ (ns)	$A_3$	$\tau_3$ (ns)	$\tau_{\text{average}}$ (ns)
0.5 M	0.63	1.26	0.15	6.68	0.22	46.99	12.13
1.0 M	0.62	1.19	0.18	6.16	0.19	42.20	9.96
1.5 M	0.65	1.09	0.20	5.73	0.15	37.92	7.54
2.0 M	0.67	0.89	0.21	5.94	0.11	31.10	5.32
2.5 M	0.71	0.56	0.19	4.11	0.09	24.22	3.40

The Fig. 5 displays a relation between the concentration of capping ligand and average PL lifetime, suggesting PL lifetime varies linearly with the concentration of the functionalizing ligand MAA.

The energy transfer from the photoexcited ensulizole to the MAA functionalized ZnCdS QDs can be envisioned by applying the FRET model. The FRET process arises due to non-radiative energy transfer absorbed by the donor fluorophore in the presence of an acceptor moiety in its proximity. As a result, the energy transfer befalls without the emission of photons due to long-range dipole-dipole interactions of transition dipoles of donor and the acceptor molecules. To study the energy transfer between ensulizole and QDs, a FRET model is employed. The overlapping between the emission spectrum of the donor and the absorption spectrum of the acceptor (Fig. 6(a)) is the basic requirement for occurrence of effective FRET process. A drop in the PL lifetime of a donor in the presence of an acceptor (Fig. 7(a)) is a quantitative measure of FRET efficiency. In the absence of the ZnCdS QDs counterpart, the average PL decay lifetime displayed by sole ensulizole is 5.09 ns. This value is reduced from 5.09 ns to 1.54 ns for an ensulizole-ZnCdS QDs dyad as exhibited by Fig. 7(b).

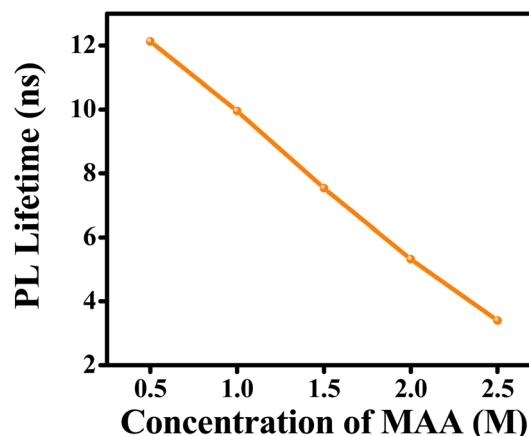


Fig. 5 Effect of concentration of capping ligand (MAA) on the average PL lifetime of ZnCdS QDs.



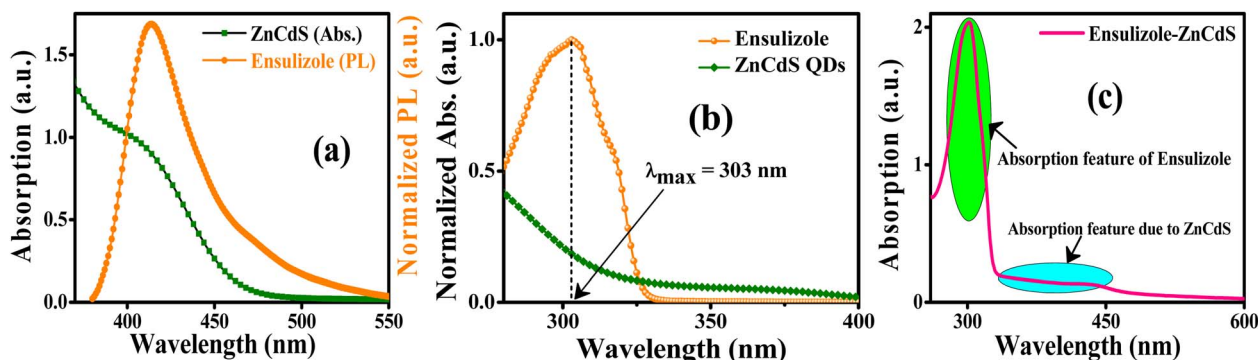


Fig. 6 (a) Spectral overlapping between the absorption spectrum of ZnCdS QDs and PL spectrum of ensulizole. (b) Normalized absorption spectrum of ensulizole and 2.5 M MAA capped ZnCdS QDs. (c) Absorption spectrum of ensulizole-ZnCdS QDs dyad containing MAA concentration 2.5 M.

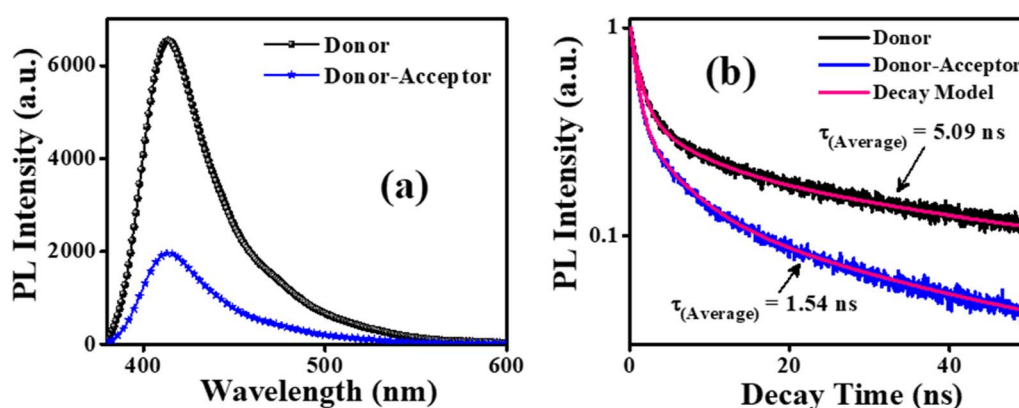


Fig. 7 (a) SSPL spectra and (b) PL decay kinetics of donor and the donor-acceptor.

The normalized absorption spectrum of ensulizole measured in the aqueous medium is displayed in Fig. 6(b) that exhibits maximum absorption at 303 nm. Fig. 6(c) displays as measured absorption spectrum of ensulizole in association with ZnCdS QDs. The presence of absorption features of both the ensulizole and the QDs is a discernible indication of the association of ensulizole with QDs. It can be assessed from Fig. 6(c) that the absorption of ensulizole at 303 nm is 2.04 and that of ZnCdS QDs is 0.15. By applying Beer-Lambert's law, the average number of ensulizole molecules associated with the 2.5 M MAA functionalized ZnCdS QDs are determined. This correspond to

$\sim 2.56 \times 10^{17}$  ensulizole molecules and  $\sim 8.01 \times 10^{16}$  number of ZnCdS QDs. Thus, the average number of experimentally determined ensulizole molecules that surround one QDs is  $\sim 3.2$ . The rate of FRET is dependent on the dipole moments of the donor and the acceptor, the refractive index of the medium, quantum yield of the donor, spectral overlap integral, orientation factor, and the distance between donor and acceptor species.<sup>53</sup> All the different FRET parameters are assessed by utilizing equations from (5) to (9) and are given in Table 2.

$$E = 1 - \frac{\tau_{\text{DA}}}{\tau_{\text{D}}} \quad (5)$$

$$E = \frac{R_0^6}{R_0^6 + r^6} \quad (6)$$

$$k_{\text{T(r)}} = \frac{1}{\tau_{\text{D}}} \left( \frac{R_0}{r} \right)^6 \quad (7)$$

$$R_0(\text{\AA}) = 0.211 \sqrt[6]{k^2 n^4 \phi_{\text{D}} J(\lambda)} \quad (8)$$

$$J(\lambda) = \int_0^\infty F_{\text{D}}(\lambda) \epsilon_{\text{A}}(\lambda) \lambda^4 d\lambda \quad (9)$$

Table 2 The FRET parameters of donor ensulizole and ensulizole-ZnCdS QDs dyad

Parameters	Values
$\tau_{\text{D}}$	5.09 ns
$\tau_{\text{DA}}$	1.54 ns
$E$	69.74%
$J(\lambda)$	$1.29 \times 10^{13} \text{ M}^{-1} \text{ cm}^{-1} \text{ nm}^4$
$R_0$	20 \AA
$R$	17.37 \AA
$k_{\text{T(r)}}$	$4.57 \times 10^8 \text{ s}^{-1}$

where,  $\tau_D$ ,  $\tau_{DA}$ ,  $R_0$ ,  $r$ ,  $\phi_D$ ,  $n$ ,  $k$ ,  $\lambda$ ,  $\epsilon_A$ ,  $J(\lambda)$  and  $k_{T(r)}$  designate average PL lifetime of the donor only, PL lifetime of donor in the presence of acceptor, Förster distance (the distance at which FRET efficiency is 50%) and the actual distance between the donor and the acceptor, fluorescence quantum yield of the donor, the refractive index of the medium, orientation factor, wavelength, absorption coefficient, spectral overlapping integral,<sup>54</sup> and non-radiative energy transfer rate, respectively.<sup>55</sup> For any randomly oriented system containing donor and acceptor species,  $k^2 = 2/3$ . The fluorescence quantum yield ( $\phi_D = 0.315$ ) of ensulizole is calculated by relative method<sup>56</sup> making use of fluorescein (in 0.1 M aqueous NaOH) as a reference fluorophore.<sup>57</sup> It is evident from eqn (5) that energy transfer ( $E$ ) exclusively depends on the difference in the PL decay lifetime of the donor–acceptor system and the sole donor.

After pulsed excitation at 306 nm, the singlet  $\pi\pi^*$  state of ensulizole is excited. The bare photoexcited ensulizole molecules dissipate absorbed UV energy through various radiative and non-radiative conduits. When an acceptor molecule in the ground state exists near the excited donor molecule, then the transition dipoles of donor and the acceptor moieties can resonate with one another. Consequently, the excited-state energy of the donor is transferred to the acceptor *via* the FRET process. The distance between the donor and the acceptor molecules must be in the range of 10–100 Å for a permissible FRET process to occur<sup>58</sup> and the donor–acceptor pair must fulfill this necessary condition. According to quantum mechanical treatment of FRET, it is an established fact that the efficacy of FRET apart from molecular structure also depends on the density of overlapping states of the donor (emissive state) and acceptor (absorption state).<sup>59,60</sup>

As ensulizole associated with 2.5 M MAA functionalized ZnCdS QDs displays a reasonable overlapping of the PL spectrum with the first excitonic peak of QDs, Fig. 6(a), suggesting the large magnitude of FRET efficiency (69.74%), Table 2, which is significantly higher than the previously reported literature values 67.3% (ref. 42) and 64.05%.<sup>44</sup> It is evident from Table 2 that MAA functionalized ZnCdS QDs coupled with ensulizole have a high value of energy dissipation through the non-radiative FRET pathway. The FRET mechanism is exceedingly distance-dependent, so it facilitates the assessment of the distance between donor and acceptor moieties. For the given FRET pair estimated values of  $E$ ,  $r$ ,  $k_{T(r)}$  and  $R_0$ , from eqn (5) to (8), respectively are summarized in Table 2. The assessed value of  $R_0$  (20 Å) is within permissible limits of 10 Å to 100 Å.<sup>61</sup> The calculated values of  $E$  (69.74%) and  $k_{T(r)}$  ( $4.57 \times 10^8 \text{ s}^{-1}$ ) specify an efficient transfer of absorbed UV energy from ensulizole to ZnCdS QDs non-radiatively. The actual donor–acceptor distance for this particular pair is  $\sim 17.37$  Å. The evaluation of all the aforementioned parameters confirms the existence of an effective FRET between ensulizole and 2.5 M MAA functionalized ZnCdS QDs.

## 4. Conclusions

To design an efficient FRET system, the spectral tuning of ternary ZnCdS QDs was performed by gradually increasing the

concentration of MAA from 0.5 to 2.5 M that led to change the bandgap from 2.88 eV to 3.37 eV in contrast to binary bare ZnS (3.62 eV) and CdS (2.42 eV) QDs. The PL spectra of these QDs revealed a shift in emission wavelength from 468 to 590 nm with a successive change in concentration of capping ligand from 0.5 to 2.5 M and this was in consistent with the results of UV-Vis measurements. A decrease in the average PL lifetime of QDs was observed with a gradual rise in the concentration of capping ligand that suggested in large-sized QDs the electron–hole pair could stay longer as compared to small-sized QDs. The effective spectral overlapping between the PL emission spectrum of ensulizole and absorption spectrum of 2.5 M MAA functionalized ZnCdS QDs, decreased the PL intensity of donor in the presence of acceptor in the dyad. The shortening of PL lifetime of the donor from 5.09 ns to 1.54 ns in the presence of acceptor, confirmed the existence of FRET between ensulizole and QDs moieties. The FRET efficiency, 69.74% was exceedingly high and confirmed an efficient FRET process was operative between ensulizole and 2.5 M MAA functionalized ZnCdS QDs. Overall, an increase of 2.44% in FRET was measured for such systems compared to previously reported literature. In future, this work can be extended to the synthesis of more biocompatible QDs and their coupling with various recommended sunscreen components for the formulation of “hybrid sunscreen” cosmetic products.

## Author contributions

All authors contributed to the writing of the manuscript and have approved the final version of the manuscript.

## Conflicts of interest

The authors declare no competing financial interest.

## Acknowledgements

The authors are highly thankful for the financial support of Higher Education Commission (HEC) Pakistan through the equipment/research grants 6976/Federal/NRPU/R&D/HEC/2017 and 20-3071/NRPU/R&D/HEC/13.

## References

- 1 X. Wang, G. Sun, N. Li and P. Chen, Quantum dots derived from two-dimensional materials and their applications for catalysis and energy, *Chem. Soc. Rev.*, 2016, **45**(8), 2239–2262.
- 2 S. Zhu, Y. Song, J. Wang, H. Wan, Y. Zhang, Y. Ning and B. Yang, Photoluminescence mechanism in graphene quantum dots: quantum confinement effect and surface/edge state, *Nano Today*, 2017, **13**, 10–14.
- 3 U. Manzoor, M. Islam, L. Tabassam and S. U. Rahman, Quantum confinement effect in ZnO nanoparticles synthesized by co-precipitate method, *Phys. E*, 2009, **41**(9), 1669–1672.



- 4 S. Shen and Q. Wang, Rational tuning the optical properties of metal sulfide nanocrystals and their applications, *Chem. Mater.*, 2013, **25**(8), 1166–1178.
- 5 S. Mukherjee, J. Selvaraj and T. Paramasivam, Ag-Doped ZnInS/ZnS Core/Shell Quantum Dots for Display Applications, *ACS Appl. Nano Mater.*, 2021, **4**(10), 10228–10243.
- 6 A. Litvin, I. Martynenko, F. Purcell-Milton, A. Baranov, A. Fedorov and Y. Gun'ko, Colloidal quantum dots for optoelectronics, *J. Mater. Chem. A*, 2017, **5**(26), 13252–13275.
- 7 D. Bimberg, M. Grundmann, F. Heinrichsdorff, N. Ledentsov, V. Ustinov, A. Zhukov, A. Kovsh, M. Maximov, Y. Shernyakov and B. Volovik, Quantum dot lasers: breakthrough in optoelectronics, *Thin Solid Films*, 2000, **367**(1–2), 235–249.
- 8 L. Etgar, P. Gao, P. Qin, M. Graetzel and M. K. Nazeeruddin, A hybrid lead iodide perovskite and lead sulfide QD heterojunction solar cell to obtain a panchromatic response, *J. Mater. Chem. A*, 2014, **2**(30), 11586–11590.
- 9 Z. Ren, J. Sun, H. Li, P. Mao, Y. Wei, X. Zhong, J. Hu, S. Yang and J. Wang, Bilayer PbS quantum dots for high-performance photodetectors, *Adv. Mater.*, 2017, **29**(33), 1702055, DOI: [10.1002/adma.201702055](https://doi.org/10.1002/adma.201702055).
- 10 X. Yin, C. Zhang, Y. Guo, Y. Yang, Y. Xing and W. Que, PbS QD-based photodetectors: future-oriented near-infrared detection technology, *J. Mater. Chem. C*, 2021, **9**(2), 417–438.
- 11 L. Duan, L. Hu, X. Guan, C. H. Lin, D. Chu, S. Huang, X. Liu, J. Yuan and T. Wu, Quantum dots for photovoltaics: a tale of two materials, *Adv. Energy Mater.*, 2021, **11**(20), 2100354, DOI: [10.1002/aenm.202100354](https://doi.org/10.1002/aenm.202100354).
- 12 F. Ma, C.-c. Li and C.-y. Zhang, Development of quantum dot-based biosensors: principles and applications, *J. Mater. Chem. B*, 2018, **6**(39), 6173–6190.
- 13 X.-L. Su and Y. Li, Quantum dot biolabeling coupled with immunomagnetic separation for detection of Escherichia coli O157: H7, *Anal. Chem.*, 2004, **76**(16), 4806–4810.
- 14 J. Britton, M. Durmuş, V. Chauke and T. Nyokong, Poly methyl methacrylate films containing metallophthalocyanines in the presence of CdTe quantum dots: non-linear optical behaviour and triplet state lifetimes, *J. Mol. Struct.*, 2013, **1054**, 209–214.
- 15 N. Zeiri, N. Sfina, S. A.-B. Nasrallah and M. Said, Linear and non-linear optical properties in symmetric and asymmetric double quantum wells, *Optik*, 2013, **124**(24), 7044–7048.
- 16 R. Maronesi, D. Ferreira, M. Lana Jr, M. Couto, S. Ferreira and A. Silva, A facile synthesis route for preparing aqueous colloidal CdS quantum dots with size-tunable optical properties, *J. Lumin.*, 2018, **202**, 489–496.
- 17 L. He, C. Luan, N. Rowell, M. Zhang, X. Chen and K. Yu, Transformations among colloidal semiconductor magic-size clusters, *Acc. Chem. Res.*, 2021, **54**(4), 776–786.
- 18 O. Micić and A. Nozik, Synthesis and characterization of binary and ternary III–V quantum dots, *J. Lumin.*, 1996, **70**(1–6), 95–107.
- 19 X. Liu, Y. Jiang, F. Fu, W. Guo, W. Huang and L. Li, Facile synthesis of high-quality ZnS, CdS, CdZnS, and CdZnS/ZnS core/shell quantum dots: characterization and diffusion mechanism, *Mater. Sci. Semicond. Process.*, 2013, **16**(6), 1723–1729.
- 20 N. Tsolekile, S. Parani, M. C. Matoetoe, S. P. Songca and O. S. Oluwafemi, Evolution of ternary I–III–VI QDs: synthesis, characterization and application, *Nano-Struct. Nano-Objects*, 2017, **12**, 46–56.
- 21 A. N. Yadav and K. Singh, Investigation of Photophysical Properties of Ternary Zn–Ga–S Quantum Dots: Band Gap versus Sub-Band-Gap Excitations and Emissions, *ACS Omega*, 2019, **4**(19), 18327–18333.
- 22 O. A. Aladesuyi and O. S. Oluwafemi, Synthesis strategies and application of ternary quantum dots—in cancer therapy, *Nano-Struct. Nano-Objects*, 2020, **24**, 100568, DOI: [10.1016/j.nanoso.2020.100568](https://doi.org/10.1016/j.nanoso.2020.100568).
- 23 R. Jose Varghese and O. S. Oluwafemi, The photoluminescence and biocompatibility of CuInS<sub>2</sub>-based ternary quantum dots and their biological applications, *Chemosensors*, 2020, **8**(4), 101, DOI: [10.3390/chemosensors8040101](https://doi.org/10.3390/chemosensors8040101).
- 24 R. J. Varghese, S. Parani, V. Remya, R. Maluleke, S. Thomas and O. S. Oluwafemi, Sodium alginate passivated CuInS<sub>2</sub>/ZnS QDs encapsulated in the mesoporous channels of amine modified SBA 15 with excellent photostability and biocompatibility, *Int. J. Biol. Macromol.*, 2020, **161**, 1470–1476.
- 25 M. Masab, H. Muhammad, F. Shah, M. Yasir and M. Hanif, Facile synthesis of CdZnS QDs: effects of different capping agents on the photoluminescence properties, *Mater. Sci. Semicond. Process.*, 2018, **81**, 113–117.
- 26 M. Yang, Y. Wang, Y. Ren, E. Liu, J. Fan and X. Hu, Zn/Cd ratio-dependent synthetic conditions in ternary ZnCdS quantum dots, *J. Alloys Compd.*, 2018, **752**, 260–266.
- 27 Y. Yao, Z. Huang, L. A. Hughes, J. Gao, T. Li, D. Morris, S. E. Zeltmann, B. H. Savitzky, C. Ophus and Y. Z. Finckel, Extreme mixing in nanoscale transition metal alloys, *Matter*, 2021, **4**(7), 2340–2353.
- 28 O. Wang, L. Wang, Z. Li, Q. Xu, Q. Lin, H. Wang, Z. Du, H. Shen and L. S. Li, High-efficiency, deep blue ZnCdS/Cd<sub>x</sub>Zn<sub>1-x</sub>S/ZnS quantum-dot-light-emitting devices with an EQE exceeding 18%, *Nanoscale*, 2018, **10**(12), 5650–5657.
- 29 C. Duan, W. Luo, T. Jiu, J. Li, Y. Wang and F. Lu, Facile preparation and characterization of ZnCdS nanocrystals for interfacial applications in photovoltaic devices, *J. Colloid Interface Sci.*, 2018, **512**, 353–360.
- 30 H.-S. Chen, S.-R. Chung, Y.-C. Chen, T.-Y. Chen, C.-Y. Liu and K.-W. Wang, The structure-dependent quantum yield of ZnCdS nanocrystals, *CrystEngComm*, 2015, **17**(27), 5032–5037.
- 31 W. Liu, H. S. Choi, J. P. Zimmer, E. Tanaka, J. V. Frangioni and M. Bawendi, Compact cysteine-coated CdSe (ZnCdS) quantum dots for in vivo applications, *J. Am. Chem. Soc.*, 2007, **129**(47), 14530–14531.
- 32 J. Chen, S. Lv, Z. Shen, P. Tian, J. Chen and Y. Li, Novel ZnCdS quantum dots engineering for enhanced visible-light-driven hydrogen evolution, *ACS Sustainable Chem. Eng.*, 2019, **7**(16), 13805–13814.





- 33 S. Qi, Y. Miao, J. Chen, H. Chu, B. Tian, B. Wu, Y. Li and B. Xin, Controlled biosynthesis of ZnCdS quantum dots with visible-light-driven photocatalytic hydrogen production activity, *Nanomaterials*, 2021, **11**(6), 1357–1372.
- 34 N. A. Monteiro-Riviere and J. E. Riviere, Interaction of nanomaterials with skin: aspects of absorption and biodistribution, *Nanotoxicology*, 2009, **3**, 188–193.
- 35 M. Mubeen, M. A. Khalid, M. Mukhtar, S. Shahrum, S. Zahra, S. Shabbir and A. Iqbal, Elucidating the photoluminescence quenching in ensulizole: an artificial water soluble sunscreen, *J. Fluoresc.*, 2021, **31**(4), 1055–1063.
- 36 A. Barth, O. Opanasyuk, T.-O. Peulen, S. Felekyan, S. Kalinin, H. Sanabria and C. A. Seidel, Unraveling multi-state molecular dynamics in single-molecule FRET experiments. I. Theory of FRET-lines, *J. Chem. Phys.*, 2022, **156**(14), 141501, DOI: [10.1063/5.0089134](https://doi.org/10.1063/5.0089134).
- 37 N. Bhattacharyya, S. Singh, D. Mukherjee, N. Das, A. Chatterjee, A. Adhikari, S. Mondal, P. Mondal, A. K. Mallick and S. K. Pal, Picosecond-resolved fluorescence resonance energy transfer (FRET) in diffuse reflectance spectroscopy explores biologically relevant hidden molecular contacts in a non-invasive way, *Phys. Chem. Chem. Phys.*, 2022, **24**(10), 6176–6184.
- 38 P. Tiwari, R. Wu, J. B. Metternich and R. Zenobi, Transition Metal Ion FRET in the Gas Phase: A 10–40 Å Range Molecular Ruler for Mass-Selected Biomolecular Ions, *J. Am. Chem. Soc.*, 2021, **143**(30), 11291–11295.
- 39 B. Wallace and P. J. Atzberger, Förster resonance energy transfer: role of diffusion of fluorophore orientation and separation in observed shifts of FRET efficiency, *PLoS One*, 2017, **12**(5), e0177122, DOI: [10.1371/journal.pone.0177122](https://doi.org/10.1371/journal.pone.0177122).
- 40 A. Kaur and S. Dhakal, Recent applications of FRET-based multiplexed techniques, *Trends Anal. Chem.*, 2020, **123**, 115777, DOI: [10.1016/j.trac.2019.115777](https://doi.org/10.1016/j.trac.2019.115777).
- 41 G. Bunt and F. S. Wouters, FRET from single to multiplexed signaling events, *Biophys. Rev.*, 2017, **9**(2), 119–129.
- 42 M. Mubeen, M. A. Khalid, M. Mukhtar, P. Sumreen, T. Gul, N. Ul Ain, S. Shahrum, M. Tabassum, A. Ul-Hamid and A. Iqbal, Elucidating the Size-dependent FRET Efficiency in Interfacially Engineered Quantum Dots Attached to PBSA Sunscreen, *Photochem. Photobiol.*, 2022, **98**, 1017–1024.
- 43 A. M. Cowden, A. L. Whittock, E. L. Holt, V. G. Stavros and M. Wills, Synthesis and characterisation of novel composite sunscreens containing both avobenzene and octocrylene motifs, *RSC Adv.*, 2023, **13**(25), 17017–17027.
- 44 M. Mubeen, M. A. Khalid, T. Gul, M. Mukhtar, A. Ul-Hamid and A. Iqbal, Cu-Enhanced Efficient Förster Resonance Energy Transfer in PBSA Sunscreen-Associated Ternary  $\text{Cu}_x\text{Cd}_{1-x}\text{S}$  Quantum Dots, *ACS Omega*, 2022, **7**(39), 35014–35022.
- 45 Y. Pu, F. Cai, D. Wang, J.-X. Wang and J.-F. Chen, Colloidal synthesis of semiconductor quantum dots toward large-scale production: a review, *Ind. Eng. Chem. Res.*, 2018, **57**(6), 1790–1802.
- 46 J. Ouyang, C. I. Ratcliffe, D. Kingston, B. Wilkinson, J. Kuijper, X. Wu, J. A. Ripmeester and K. Yu, Gradiently Alloyed  $\text{Zn}_x\text{Cd}_{1-x}\text{S}$  Colloidal Photoluminescent Quantum Dots Synthesized via a Noninjection One-Pot Approach, *J. Phys. Chem. C*, 2008, **112**(13), 4908–4919.
- 47 A. Yeltik, S. Delikanli, M. Olutas, Y. Kelestemur, B. Guzel Turk and H. V. Demir, Experimental determination of the absorption cross-section and molar extinction coefficient of colloidal CdSe nanoplatelets, *J. Phys. Chem. C*, 2015, **119**(47), 26768–26775.
- 48 S. Mohamed, M. Awad and M. Shaban, Optical constants, photoluminescence and thermogravimetry of ZnS–ZnO hybrid nanowires synthesized via vapor transport, *Appl. Phys. A*, 2022, **128**(4), 1–7.
- 49 M. Islam, M. Hossain, M. Aliyu, P. Chelvanathan, Q. Huda, M. Karim, K. Sopian and N. Amin, Comparison of structural and optical properties of CdS thin films grown by CSVT, CBD and sputtering techniques, *Energy Procedia*, 2013, **33**, 203–213.
- 50 X. Zhong, Y. Feng, W. Knoll and M. Han, Alloyed  $\text{Zn}_x\text{Cd}_{1-x}\text{S}$  nanocrystals with highly narrow luminescence spectral width, *J. Am. Chem. Soc.*, 2003, **125**(44), 13559–13563.
- 51 M. Khawla, H. Zouhour, C. Yves, H. Souhaira and M. Rym, ZnS quantum dots as fluorescence sensor for quantitative detection of tetracycline, *Opt. Mater.*, 2022, **125**, 112103, DOI: [10.1016/j.optmat.2022.112103](https://doi.org/10.1016/j.optmat.2022.112103).
- 52 C. H. Wang, T. Te Chen, Y. F. Chen, M. L. Ho, C. W. Lai and P. T. Chou, Recombination dynamics in CdTe/CdSe type-II quantum dots, *Nanotechnology*, 2008, **19**(11), 115702, DOI: [10.1088/0957-4484/19/11/115702](https://doi.org/10.1088/0957-4484/19/11/115702).
- 53 V. K. Komarala, A. L. Bradley, Y. P. Rakovich, S. J. Byrne, Y. K. Gun'ko and A. L. Rogach, Surface plasmon enhanced Förster resonance energy transfer between the CdTe quantum dots, *Appl. Phys. Lett.*, 2008, **93**(12), 123102, DOI: [10.1063/1.2981209](https://doi.org/10.1063/1.2981209).
- 54 M. C. Dos Santos, W. R. Algar, I. L. Medintz and N. Hildebrandt, Quantum dots for Förster resonance energy transfer (FRET), *Trends Anal. Chem.*, 2020, **125**, 115819, DOI: [10.1016/j.trac.2020.115819](https://doi.org/10.1016/j.trac.2020.115819).
- 55 S. A. Raza, S. Q. Naqvi, A. Usman, J. R. Jennings and Y. W. Soon, Spectroscopic study of the interaction between rhodamine B and graphene, *J. Photochem. Photobiol., A*, 2021, **418**, 113417, DOI: [10.1016/j.jphotochem.2021.113417](https://doi.org/10.1016/j.jphotochem.2021.113417).
- 56 C. Würth, M. Grabolle, J. Pauli, M. Spieles and U. Resch-Genger, Relative and absolute determination of fluorescence quantum yields of transparent samples, *Nat. Protoc.*, 2013, **8**(8), 1535–1550.
- 57 M. Mubeen, M. A. Khalid, S. Shahrum, M. Mukhtar, P. Sumreen, M. Tabassum, A. Ul-Hamid, M. A. Nadeem and A. Iqbal, Exploring the photoexcited electron transfer dynamics in artificial sunscreen PBSA-coupled biocompatible ZnO quantum dots, *New J. Chem.*, 2022, **46**, 9526–9633.
- 58 B. Masters, Paths to Förster's resonance energy transfer (FRET) theory, *Eur. Phys. J. H*, 2014, **39**(1), 87–139.



- 59 D. Abramavicius, B. Palmieri, D. V. Voronine, F. Sanda and S. Mukamel, Coherent multidimensional optical spectroscopy of excitons in molecular aggregates; quasiparticle versus supermolecule perspectives, *Chem. Rev.*, 2009, **109**(6), 2350–2408.
- 60 X. Wang, Z. Zhang and J. Wang, Excitation-energy transfer under strong laser drive, *Phys. Rev. A*, 2021, **103**(1), 013516, DOI: [10.1103/PhysRevA.103.013516](https://doi.org/10.1103/PhysRevA.103.013516).
- 61 X. Ji, W. Wang and H. Mattoussi, Controlling the spectroscopic properties of quantum dots via energy transfer and charge transfer interactions: concepts and applications, *Nano Today*, 2016, **11**(1), 98–121.

